Electronic Supplementary Material (ESI) for RSC Advances.
This journal is © The Royal Society of Chemistry 2015

Electronic Supplementary Information (ESI)

Sol-gel based simonkolleite nanopetals with SnO_2 nanoparticles in graphite-like amorphous carbon as efficient and reusable photocatalyst

Moumita Pal, Susanta Bera and Sunirmal Jana*

Sol-Gel Division
CSIR–Central Glass and Ceramic Research Institute (CSIR–CGCRI)
196 Raja S.C. Mullick Road, P.O. Jadavpur University, Kolkata –700032, India
*Corresponding author: Tel.: +91 33 23223303, Fax: +91 33 2473 0957
E-mail address: sjana@cgcri.res.in, janasunirmal@hotmail.com (S. Jana)

C-O-N-T-E-N-T-S

Table S1: *Details of samples*

Designation			**Curing atmosphere** *[air / vacuum (-1 bar pressure) / pure oxygen gas]*	**System**
Sol	*Gel*	*Nanocomposite*		
ZSS-LC	ZSG-LC	ZSV-LC	Under vacuum at 450^{o}C	Simonkolleite–SnO_2–Carbon
ZSS	ZSG	ZSV		
ZSS-HC	ZSG-HC	ZSV-HC		
ZSS	ZSG	ZSA	In air at 450^{o}C	Zinc oxychloride–SnO_2
ZS/S	ZS/G	ZS/V	Under vacuum at 450^{o}C followed by curing in pure oxygen gas at 400^{o}C	Simonkolleite–SnO_2 –Zinc oxychloride
SS	SG	SV	Under vacuum at 450^{o}C	SnO_2–Carbon
ZS	ZG	ZV	Under vacuum at 450^{o}C	Simonkolleite–ZnO–Carbon

Note: ZS/S *sol was identical Zn to Sn atomic ratio (2 : 1) as well as total equivalent oxide weight percentage (4 wt%) with ZSS sol. However, no acetylacetone was added in the* ZS/S *precursor sol.*

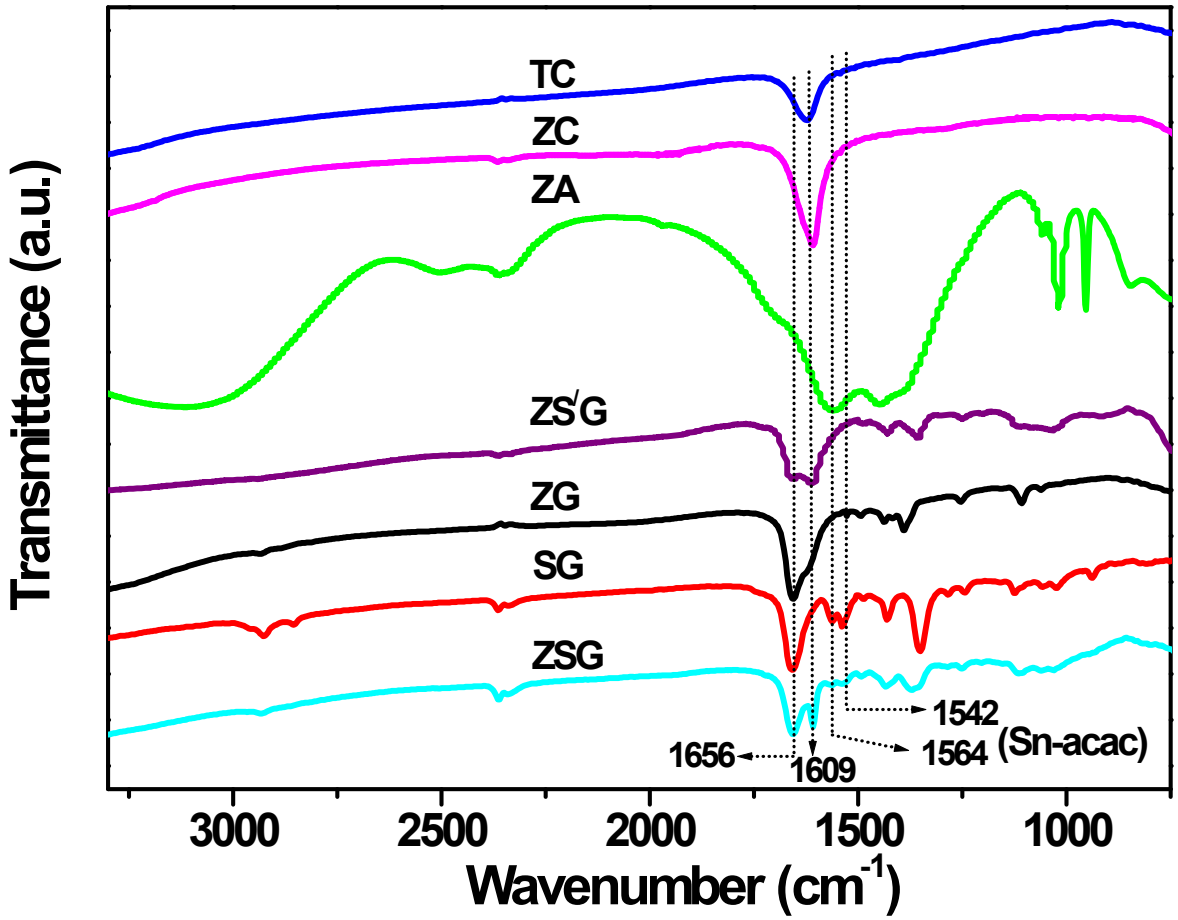

Fig. S1: *FTIR spectra of ZSG, ZS/, ZG and SG gels cured at 130±5°C for 2 h in air along with the precursor materials (zinc acetate dihydrate, ZA; zinc chloride, ZC; tin (IV) chloride pentahydrate, TC).*

Table S2: *Assignment of FTIR vibrations from Figure S1*

Vibration (cm^{-1})	***Assignment***	***Reference***
2925, 2856	CH_3, CH_2 stretching vibrations	[1]
1656, 1610	O-H bending vibrations	[2], [3]
1564	$\nu_{C=O}$ vibration [actylacetonate complexed with Sn(IV)]	[4]
1542	$\nu_{C=C}$ + $\nu_{C=O}$ vibrations [actylacetonate complexed with Sn(IV)]	
1460	Bending vibration, $-CH_2$ / asymmetric stretching, $-CH_3$	[5]
1438	Asymmetric bending vibration, $-CH_3$	
1431	$-CH_2$ deformation	[6]
1377	$-OC_2H_4$ group	[5]
1350	Symmetric bending vibration, $-CH_3$ / stretching vibration, $-CH_2$	
1254	C-O-H vibration	[7]
1233	$-CH_2$ twisting	[5]
1198	Stretching vibration, –C–C–	[8]
1120	Stretching vibration, C–O–C	[5]
1060	Stretching, vibration –C–OH	[5]
1024	Stretching vibration, –C–OH / C–O–C	
1010	Stretching vibration, $-OCH_3$	[9]
940	Stretching vibration, –C–C–/ CO / $-CH_3$ rocking vibration	[5]
890	$-OC_2H_4$ rocking vibration	
835	Asymmetric bending vibration, $-CH_3$	

References:

1 D.R.U. Knappe, L. Li. P.A. Quinlivan and T.B. Wagner, American Water Work Association Research Foundation Research Report No. 90926, 2003.

2 Z. M. El-Bahy, *Mod. Res. Catal.,* 2013, **2**, 136-147.

3 R. L. Frost, B. J. Reddy, and E. C. Keeffe, *Transition Met. Chem.*, 2009, **34,** 23-32.

4 R.L. Frost, W.N. Martens, P. Williams and J.T. Kloprogge, *Mineral. Mag.*, 2002, 66, 1063-1073.

5 T. T. Nguyen, I. M. Raupach and L. J. Janik, *Clays Clay Miner.,* 1987, **35**, 60-67.

6 P. Mani and S. Suresh, *Rasayan J. Chem.,* 2009, **2,** 340-344.

7 G.C. Trivino, O.G. Guzman and J.G. Contreras, *J. Chil. Chem. Soc.,* 2006, **51**, 989-992.

8 D. A. Rexalin, *Cauvery Res. J.*, 2007, **1**, 75-81.

9 J. H. Deshmukh and M. N. Deshpande, *Chem. Environ. Pharm. Res.,* 2011, **2**, 20-25.

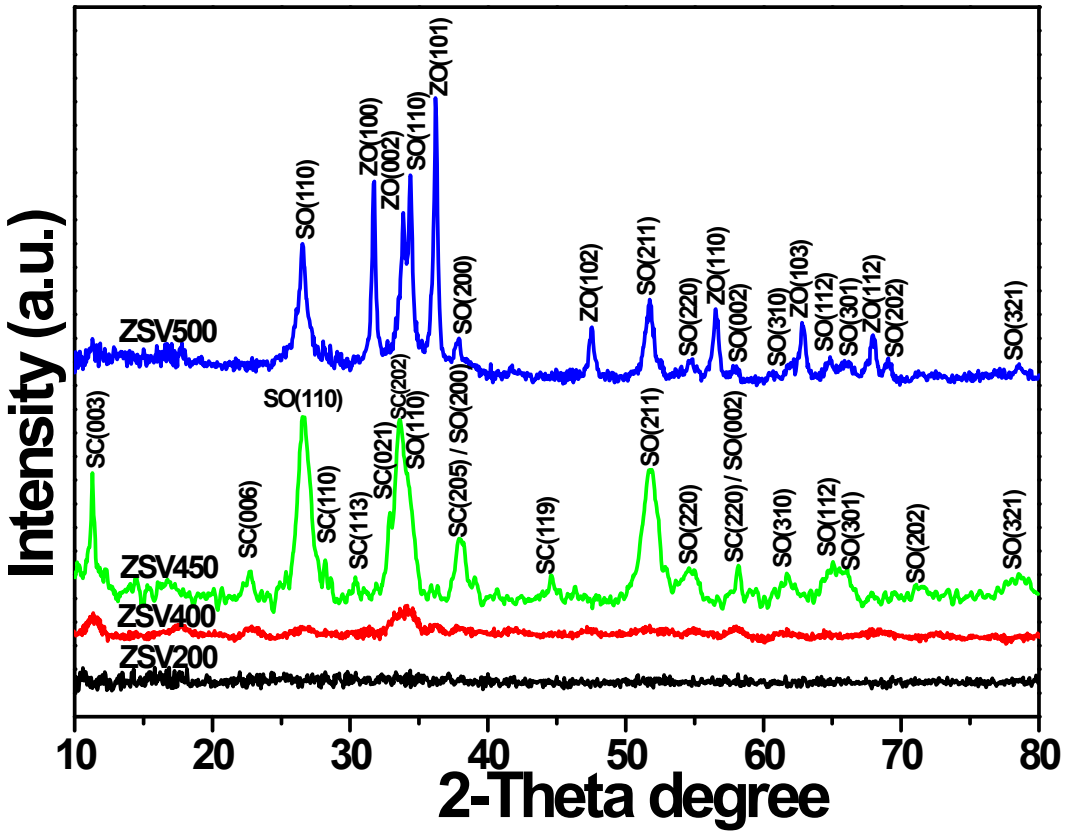

Fig. S2: *XRD patterns of ZSG gel cured at different temperatures under vacuum (-1 bar pressure).* As seen from **Figure S1**, the ZSG gel cured at 400°C is semicrystalline as evident from the intensity of XRD patterns but the gel becomes highly crystalline after curing at 450°C under the vacuum. The XRD patterns are well matched with rhomboherdal simonkolleite [r-SC, JCPDS Card 07-0155] and tetragonal tin oxide (t-SnO_2, JCPDS Card 41-1445]. It is very interesting to note that on further increasing the curing temperature to 500°C, the simonkolleite fully dissociates to hexagonal zinc oxide (h-ZnO) [JCPDS Card 36-1451] as evident from the XRD patterns of the sample.

Proposed chemical reactions for formation of different products from ZSG gel on thermal curing at different temperatures and in different atmospheres

2-Methoxy ethanol (ROH, b.pt. 124-125^{o}C; R = -$C_2H_4OCH_3$) is a clear, colourless liquid with ether-like odour. It is in the class of glycol ethers which can able to dissolve different types of chemical compounds and is miscible with water and other solvents [1]. Moreover, several metal/metal ions would co-ordinate/solvate with ROH [2,3]. In this work, from FTIR spectral result (**Fig. S2 and Table S2**) of 130^{o}C (above the b.pt. of ROH) cured gels, it is seen that ROH is present in the gels. It is important to note that the presence of FTIR vibration at 1254 cm^{-1} (assigned as C-O-H vibration of ROH) particularly in Zn^{2+} containing gels would indicate an interaction exist between ROH and the metal ions [3]. It is also noted that no free acetylacetone or complexed acac of Zn^{2+} is detected from FTIR spectral study of 130^{o}C cured gels. This would be due to very low precursor sol pH (<1) [4]. However, there is an evidence of complexation of acac with Sn^{4+} as observed from FTIR spectra of the tin gels (ZSG, ZS/V and SV). Therefore, on the basis of FTIR study on 130^{o}C cured gels and subsequently, the structural characterizations by XRD patterns (**Fig. 1**) as well FESEM (**Fig. 5**) and TEM (**Fig. 6**), Raman spectra (**Fig. 2**) and XPS analyses (**Fig. 3**) of the cured gels at different temperatures and in different atmospheres, the following chemical equations [4,6] (Eqns. 1–7) have been proposed. It is known that curing the metal-organics under vacuum can generate carbon [5] vis-à-vis metal based compounds. Therefore, the source of carbon in the vacuum cured gels as evident from Raman, XPS and HR-TEM analyses would be the organics (i.e. metal ions co-ordinated/solvated with ROH/acac) in the precursor gels.

$$SnCl_4 \xrightarrow{xROH + yH_2O;\ R = -C_2H_4OCH_3} Sn(OR)_x(OH)_y(Cl)_{4-x-y} + xHCl \quad \text{-- (1)}$$

$$Sn(OR)_x(OH)_y(Cl)_{4-x-y} \xrightarrow{xacac} Sn(acac)_x(OH)_y(Cl)_{4-x-y} + xROH \quad \text{-- (2)}$$

$$Sn(acac)_x(OH)_y(Cl)_{4-x-y} \xrightarrow{400^{o}C,\ Vacuum} SnO_2 + HCl + H_2O + C/C\ oxides \quad \text{-- (3)}$$

$$Zn(ac)_2 + (2-m-n)H_2O \xrightarrow{mROH + nHCl + (2-m-n)H_2O} Zn(OH)_{2-m-n}(OR)_m(Cl)_n + 2AcH \quad \text{-- (4)}$$

$$Zn(OH)_{2-m-n}(OR)_m(Cl)_n \xrightarrow{400^{o} - 500^{o}C,\ Vacuum} Zn_5(OH)_8Cl_2 \cdot H_2O + C/C\ oxides \quad \text{-- (5)}$$

$$Zn_5(OH)_8Cl_2 \cdot H_2O \xrightarrow{500^{o}C,\ Vacuum} 5ZnO + 2HCl + 4H_2O \quad \text{-- (6)}$$

$$Zn(OH)_{2-m-n}(OR)_m(Cl)_n \xrightarrow{450^{o}C,\ Air} ZnO.ZnCl_2.H_2O + H_2O + C/C\ oxides \quad \text{-- (7)}$$

Note: x, y, m and n are positive integers; ROH = 2-methoxy ethanol; C = carbon; acac = acetylacetonate group; ac = acetate group; AcH = acetic acid, C oxides = oxides of carbon]

1 http://shodhganga.inflibnet.ac.in/bitstream/10603/12322/14/15_chapter%203.pdf

2 R. Castaneda, S. Draguta, A. Yakovenko, M. Fonari and T. Timofeeva, *Acta Crystallogr. Sect. E: Struct. Rep. Online,* 2014, **E70**, m164-m165.

3 R. L. Frost, B. J. Reddy, and E. C. Keeffe, *Transition Met. Chem.,*2009, **34,** 23-32.

4 M. Pal, S. Bera and S. Jana, *J. Sol-Gel Sci. Technol*.,2013,**67**, 8-17.

5 C. Klinke and K. Kern, *Nanotechnology,* 2007, **18**, 215601, 4 pages.

6 W. Zhang and K. Yanagisawa, *Chem. Mater.,* 2007, **19,** 2329-2334.

Table S3: *Carbon content (measured by carbon determinator) of samples cured at 450°C under vacuum*

Sample	**Carbon content (±0.5%)**
ZSV-LC	9.9
ZSV	17.9
ZSV-HC	23.5
ZV	6.6
SV	17.3

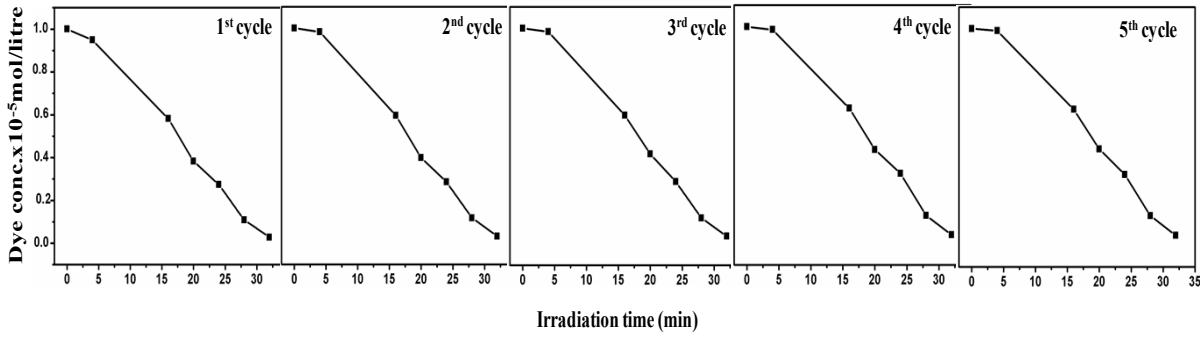

Fig. S3: *Plots of remnant dye concentration versus UV illumination time for successive recycles using ZSV as photocatalyst. The percent decomposition of the dye for the five successive cycles is given in Table S3.*

Table S4: *1st cycle photocatalytic activity of different samples*

Sample	***Percentage of dye decomposition at different illumination time (min) of UV***							***Dye decomposition rate constant ($x10^{-3}$ min^{-1})***
	20	***24***	***28***	***32***	***50***	***80***	***100***	
ZSV	68.0	78.1	92.7	~100.0	---	---	---	96.1
ZS/V	27.1	---	---	37.1	---	63.9	84.3	14.5
ZSA	7.1	---	---	---	18.6	30.0	47.7	4.5
ZV	7.1	---	---	---	17.1	31.4	41.4	4.1
SV	5.7	---	---	---	10.1	20.7	30.9	1.0

Table S5: *Performance of ZSV photocatalyst after successive recycles*

Cycle No.	***Percentage of dye decomposition after 32 min of UV exposure***
1st	99.98
2nd	96.85
3rd	96.46
4th	95.35
5th	94.95

Table S6: *Crystallite sizes of t-SnO_2 and r-SC in different samples measured from their XRD patterns*

Sample designation	**t-SnO_2 [along (110) plane)]**	**r-SC [along (003) plane)]**
	Crystallite size (nm)	*Crystallite size (nm)*
ZSV	11.6±0.5	29.4±0.8
ZS/V	7.0±0.2	33±1.3
ZSA	7.8±0.4	-----
SV	14.3±1.0	-----

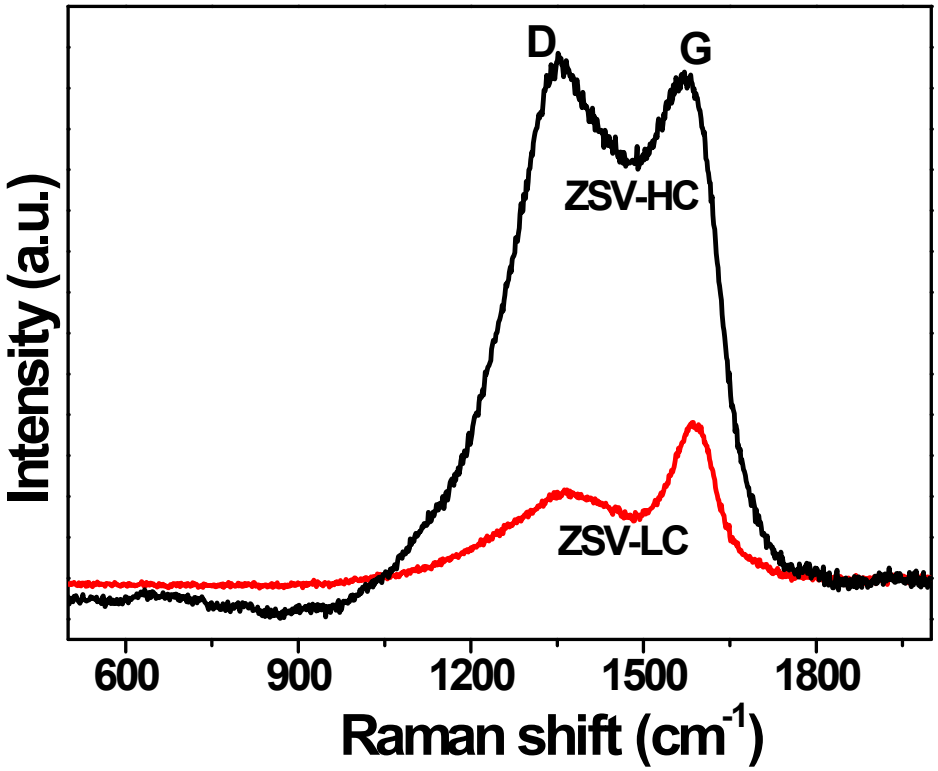

Fig. S4: *Raman spectra of ZSV-LC and ZSV-HC*

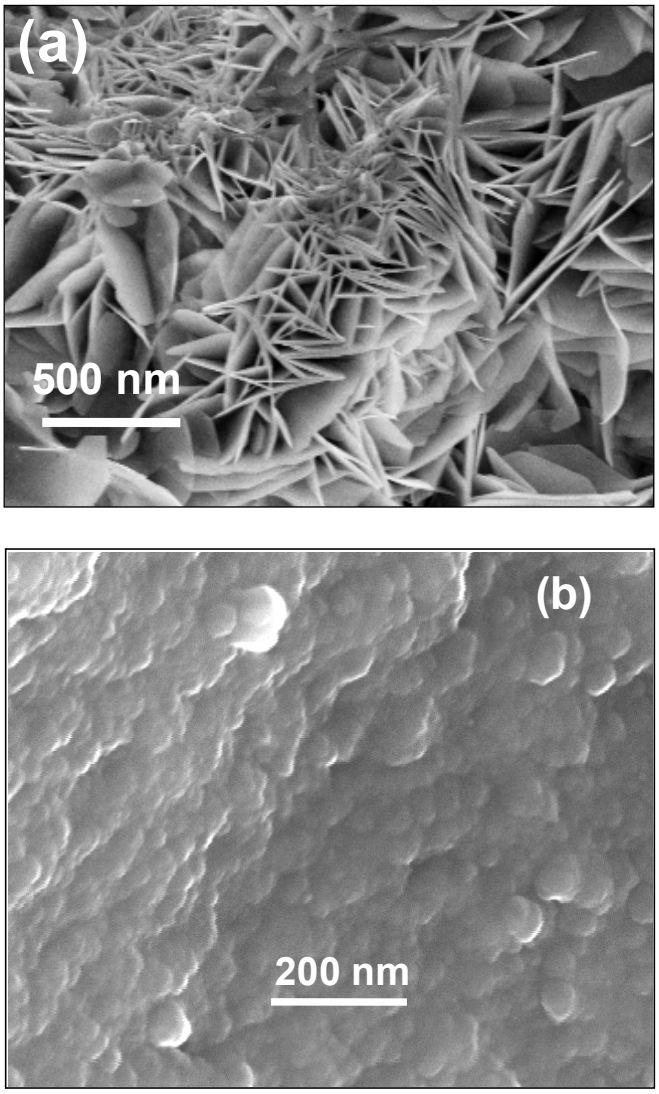

Fig. S5: *FESEM images of (a) ZS/V and (b) SV samples.* Surface microstructure of ZS/V sample shows the presence of nanopetals (thickness, 27-33 nm), considered to be simonkolleite. The SV sample shows spherical shaped nanoclusters (size, 17±2 nm).

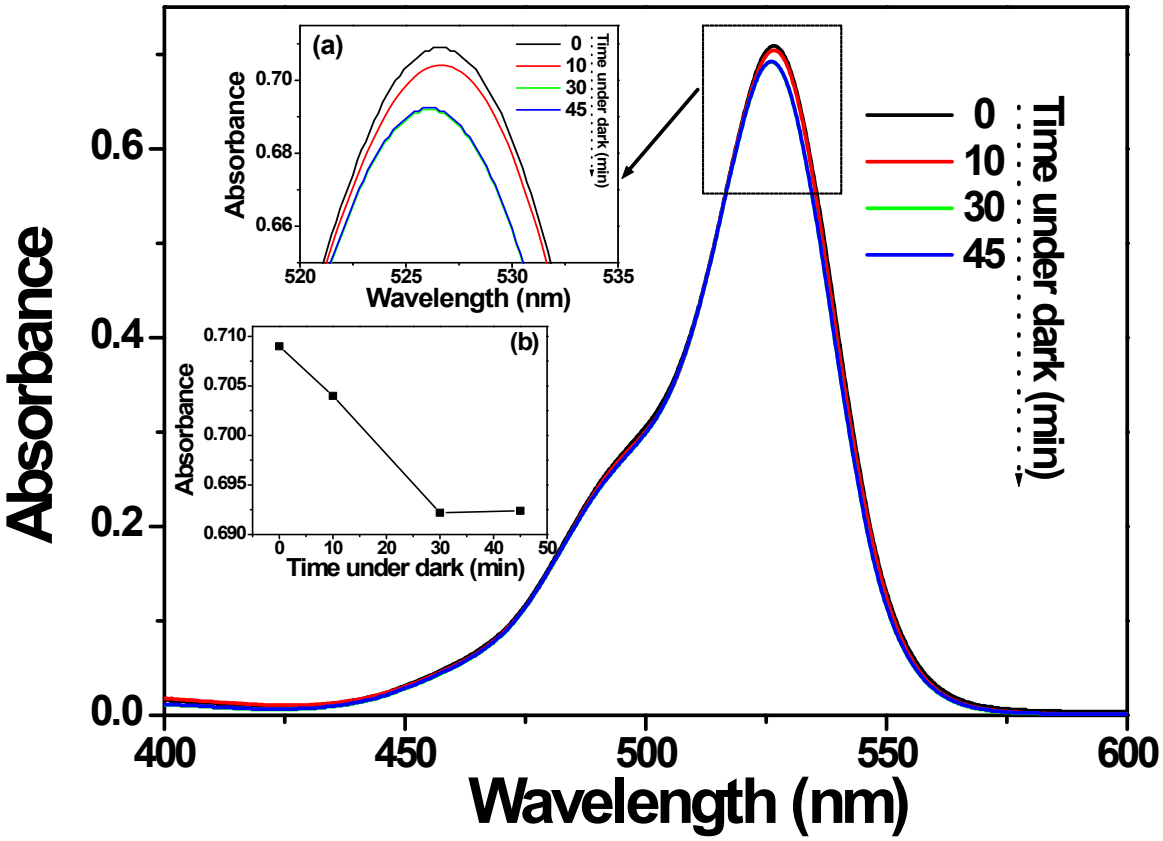

Figure S6: *Absorption spectra of Rh 6G dye solution in presence ZSV sample under dark condition at different times. Inset (a) shows the enlarged marked portion of the spectra whereas inset (b) displays the change of absorbance due to adsorption of the dye at different times under the dark condition without UV irradiation.*

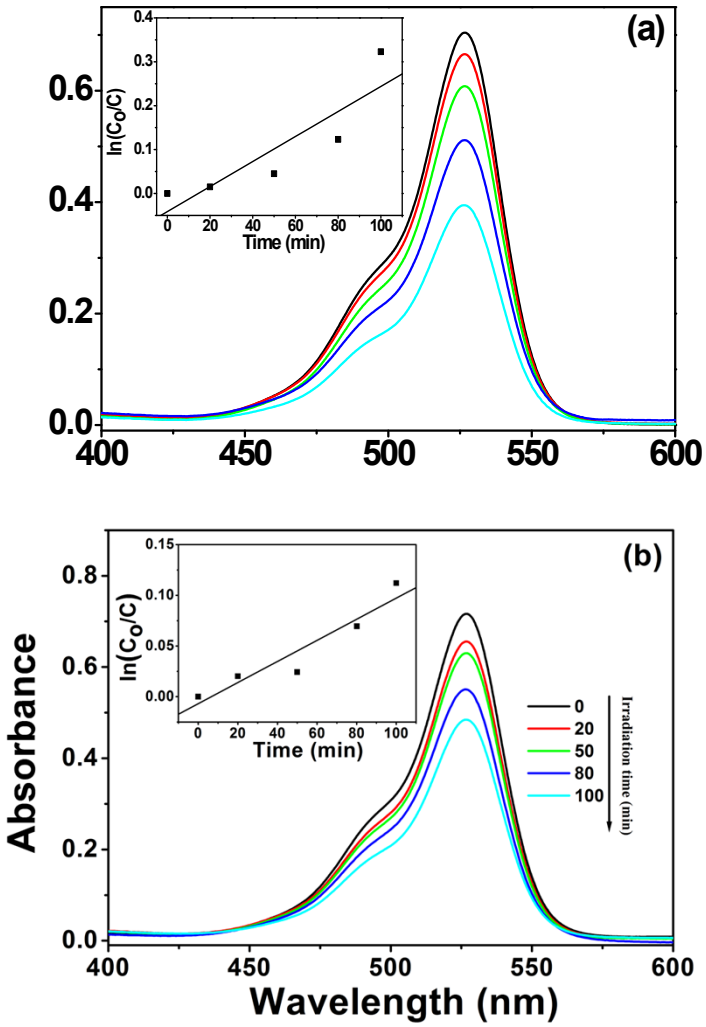

Fig. S7: *Visible spectra, (a) and (b) of dye solution at different time of UV illumination using the photocatalysts, ZV and SV, respectively (insets show the determination of respective dye decomposition rate constant, considering first order reaction kinetics).*

Table S7: *Photodecomposition of rhodamine 6G dye using different photocatalysts [1-7].*

Photocatalyst	**Dye concentration x 10^{-5} (M)**	**Time taken for complete dye decomposition (min)**	**Rate constant (min^{-1})**	**Reference**
Ca_2SmBiO_6	9.6	100	0.0348	[1]
Anatase TiO_2–SiO_2 nanocomposites	2.5	90	0.0735	[2]
TiO_2	1.5	35	0.032	[3]
ZnO nanowire/reduced graphene oxide nanocomposites	2.08	10 (98% dye decomposed)	- - - -	[4]
Au-CdSe penta pod heterostructures	0.218	150	0.013	[5]
New sol-gel nanocomposite: Simonkolleite nanopetals – quasi spherical tin oxide nanoparticles embedded in graphite-like amorphous carbon	**1.0**	**32**	**0.096**	**[Present work]**

References:

[1] S. Feraru, A.I. Borhan, P. Samoila, C. Mita, S. Cucu-Man, A.R. Iordan and M.N. Palamaru, *J. Photochem. Photobio. A Chem.,* 2015, **307-308**, 1-8.

[2] W. Dong, Y. Sun, Q. Ma, L. Zhua, W. Hua, X. Lu, G. Zhuang, S. Zhang, Z. Guo and D. Zhao, *J. Hazard. Mater.* 2012, **229-230,** 307-320.

[3] A. Mills, A. Belghazi, R. H. Davies, D. Worsley and S. Morris *J. Photochem. Photobio. A Chem.,* 1994,**79,** 131-139.

[4] C. Zhang, J. Zhang, Y. Su, M. Xu, Z. Yang and Y. Zhang, *Physica E*, 2014, **56**, 251-255.

[5] K. K. Haldar, G. Sinha, J. Lahtinen, and A. Patra, *ACS Appl. Mater. Interfaces,* 2012, **4**, 6266-6272.

Electrochemical impedance spectroscopy (EIS) study on different photocatalysts [1-8]:

Several authors utilized EIS tool to explain the photocatalytic activity of semiconductors including carbon coupled single / mixed metal oxide nanocomposites. Among them some important works especially on carbon based composite materials are given below. The C_{60} hybridized ZnO photocatalyst with varying carbon content prepared by Fu *et al.* **[1]** also showed smallest arc radius on the EIS Nyquist plot which revealed that an effective separation of the photogenerated electron-hole pair along with a fast interfacial charge transfer to the electron donor/electron acceptor. They also observed that the order of arc radius was resembled with the order of photocatalytic activities. To explain an improved photocatalytic activity of graphene hybridized ZnO, Xu *et al.* **[2]** also took the help of EIS responses of the electrode sample. Nynquist plot of the sample shows smaller arc radius than ZnO, indicating a fast interfacial charge transfer to the electrode donor/electron acceptor. Wang *et al*. **[3]** also prepared ZnO/reduced graphene oxide (rGO)/CdS heterostructures. The authors observed that the heterostructures posses smallest arc radius in EIS plane that could be the reason for the effective separation of photoinduced electron–hole pairs and faster interfacial charge transport in the sample. In this study, they found that the rGO interlayer plays an important role in promoting photo generated charge transfer which consequences an enhancement of the charge separation efficiency. Yu *et al.* **[4]** reported efficient photocatalytic activity of TiO_2-CNT heterojunctions with an optimum thickness of TiO_2 layer due the faster electron transfer as revealed from the lowest impedance arc radius of the sample. Synthesis of a novel nanocomposite from carbon quantum dots (CQDs) and TiO_2 nanotubes (CQDs/TiO_2) was reported by Sun *et al* **[5]**. They explained an enhanced photocatalytic activity of the nanocomposite on the basis of the smaller resistance value compare to TiO_2 in EIS measurement. Wang *et al.* **[6]** fabricated a photocatalytically efficient composite Cu_2O/TiO_2/carbon aerogel electrode having good conductivity, shows electrochemical impedance of 17Ω. Preparation of a magnetically recyclable and high efficiency $NiFe_2O_4$/ MWNT ($NiFe_2O_4$/MWNT) photocatalyst was reported. EIS study of $NiFe_2O_4$ and $NiFe_2O_4$/MWNT(0.30) under UV irradiation showed that the arc radius of $NiFe_2O_4$/MWNT(0.30) is smaller than that of $NiFe_2O_4$, indicating that a more effective separation of photogenerated electron-hole pairs along with a faster interfacial charge transfer could occur in $NiFe_2O_4$/MWNT(0.30) [**7**]. On the other hand, Ansari *et al.* **[8]** synthesized pure SnO_2 and Ag-SnO_2 nanocomposites using an electrochemically active biofilm. The arc radius of the EIS Nyquist plots of the Ag-SnO_2 nanocomposite was found to be smaller than that of pure SnO_2 in the dark and under visible light irradiation, implying a faster interfacial charge transfer took place at the Ag-SnO_2 photocatalyst surface. The details on the rate of decomposition on the various organics using different photocatalysts are summarized in **Table S8**.

Table S8: *Electrochemical impedance spectroscopy (EIS) study on different photocatalysts [1-8].*

Photocatalyst system	***Organics***	***Decomposition rate constant of organics (k, min^{-1})***	***Reference***
C_{60} hybridized ZnO	Methylene blue	0.0569	[1]
Graphene hybridized ZnO	Methylene blue	0.098	[2]
ZnO/rGO/CdS heterostructures	Methylene blue	0.006	[3]
TiO_2-CNT heterojunction	Phenol	0. 0125	[4]
Carbon QDs / TiO_2 nanotube	Methylene blue	35% degraded after 100 min	[5]
Cu_2O/TiO_2/carbon aerogel	2,4,6-trichlorophenol	96.3% decomposed at 5.5 h	[6]
$NiFe_2O_4$/MWCNT	Phenol	0.00468	[7]
Ag-SnO_2	Methyl orange	~0.00396	[8]
	Methylene blue	~0.00483	
	4-Nitrophenol	~0.00193	
	2-Chlorophenol	~0.00186	
New sol-gel nanocomposite: Simonkolleite nanopetals – quasi spherical tin oxide nanoparticles embedded in graphite-like amorphous carbon	**Rh 6G**	**0.096**	**[Present work]**

References:

[1] H. Fu, T. Xu, S. Zhu, and Y. Zhu, *Environ. Sci. Technol.,* 2008, **42***,* 8064-8069.

[2] T. Xu, L. Zhang, H. Cheng and Y. Zhu, *Appl. Catal. B Environ.,* 2011, **101**, 382-387.

[3] Y. Wang, F. Wang and J. He, *Nanoscale*, 2013, 2013, **5**, 11291–11297.

[4] H. Yu, X. Quan, S. Chen, H. Zhao and Y. Zhang, *J. Photochem Photobio A Chem.,* 2008, **200**, 301-306.

[5] M. Sun, X. Ma, Xi Chen, Y. Sun, X. Cui and Y. Lin, *RSC Adv.,* 2014, **4**, 1120-1127.

[6] Y. Wang, Y. Zhang, G. Zhao, H. Tian, H. Shi, and T. Zhou, *ACS Appl. Mater. Interfaces,* 2012, **4**, 3965-3972.

[7] P. Xiong, Y. Fu, L. Wang and X. Wang, *Chem. Eng. J.*, 2012, **195-196**, 149-157.

[8] S. A. Ansari, M. M. Khan, M. O. Ansari, J. Lee and M. H. Cho, *RSC Adv.,* 2014, **4**, 26013-26021.

Table S9: *Surface area of some carbon coupled photocatalysts [1-4]*

Description of photocatalyst	**Surface area** (m^2/g)	**Reference**
C_{60}-ZnO	56.9	[1]
CoS_2-C_{60}/TiO_2	43.58	[2]
TiO_2/graphene	62.0	[3]
C_{60}/TiO_2	82.7	[4]
New sol-gel nanocomposite: Simonkolleite nanopetals – quasi spherical tin oxide nanoparticles embedded in graphite-like amorphous carbon	**143.0**	**[Present work]**

References:

1 H. Fu, T. Xu, S. Zhu and Y. Zhu, *Environ. Sci. Technol.,* 2008**, 42**, 8064–8069.

2 M. Zeda, O. Wonchun, *Chinese J. Catal.* 2012, **33**, 1495–1501.

3 Z. Peining, A. S. Nair, P. Shengjie, Y. Shengyuan and S. Ramakrishna, *ACS Appl. Mater. Interfaces,* 2012, **4**, 581-585.

4 Y. Long, Y. Lu, Y. Huang, Y. Peng, Y. Lu, S.-Z. Kang and J. Mu, *J. Phys. Chem. C*, 2009, **113**, 13899-13905.

Table S10: *Photodecomposition rate constant (first order) of different organic compounds [1-4].*

Photocatalyst	**Organic compound**	**Rate constant, k (min^{-1})**	**Light source**	**Reference**
TiO_2 nanoparticles	Acetone	~0.005	UV lamp (λ = 365 nm, 15 W)	[1]
TiO_2 nanofibers / nanotubes	Methylene blue	~0.029	Mercury lamp (λ = 320-400 nm, λ_{max} = 365 nm; 160 W)	[2]
Ag and anatase TiO_2	Methyl orange	~0.001	Metal halogen desk lamp (300 W)	[3]
	Dichlorophenol	~0.019		
Ag–SnO_2 nanocomposites	Methyl orange	~0.004	Lamp (λ> 400 nm, 400 W)	[4]
	Methylene blue	~0.005		
	4-Nitrophenol	~0.002		
	2-Chlorophenol	~0.0019		
New sol-gel nanocomposite: Simonkolleite nanopetals – quasi spherical tin oxide nanoparticles embedded in graphite-like amorphous carbon	**Rhodamine 6G**	**~0.096**	**UV (λ = 254 nm; 8 W)**	**[Present work]**

References:

1. J. C. Yu, J. Yu, W. Ho and L. Zhang, *Chem. Commun.*, 2001, 1942-1943.
2. J. Wang, J. Hou, M. W. Ellis and A. S. Nain, *New. J. Chem.,* 2013, **37**, 571-574.
3. J. Virkutyte and R. S. Varma, *RSC Adv*., 2012, **2**, 2399-2407.
4. S. A. Ansari, M. M. Khan, M. O. Ansari, J. Lee and M. H. Cho, *RSC Adv.,* 2014, **4,** 26013-26021.

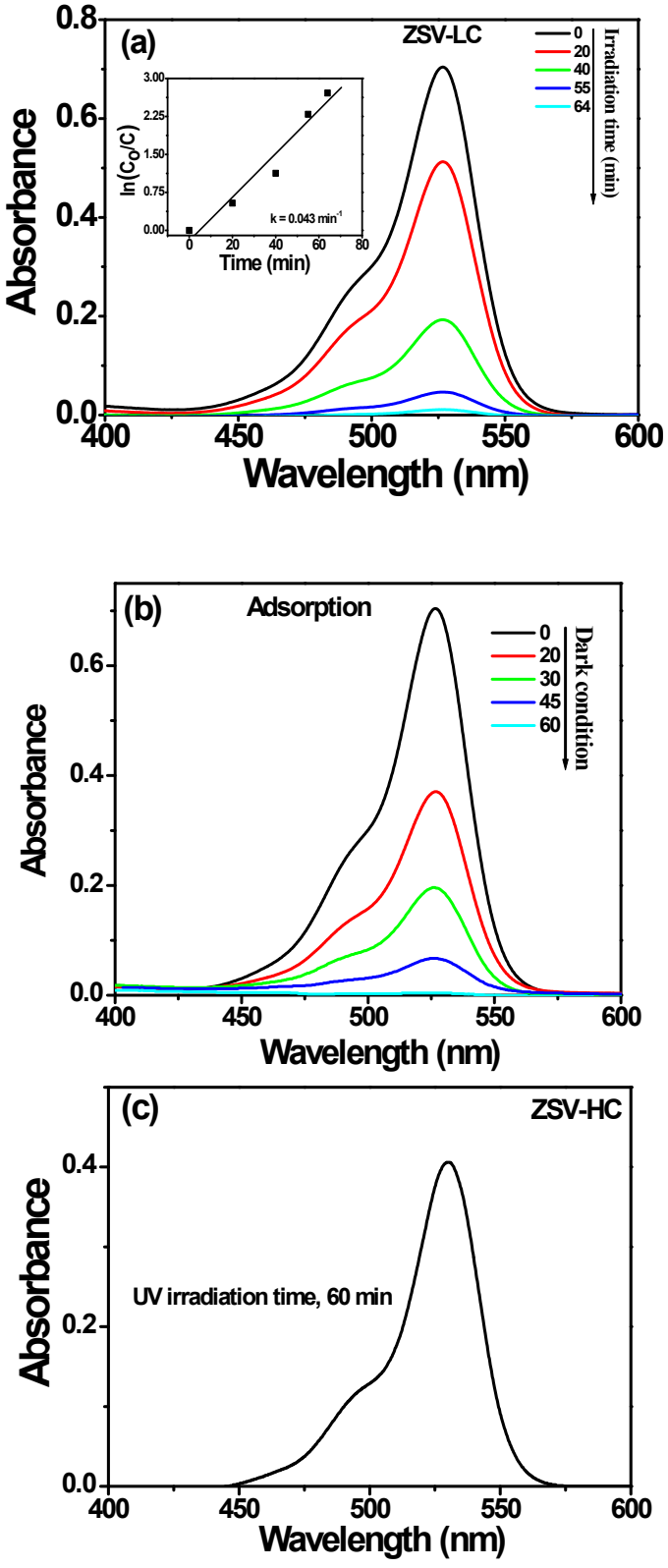

Fig. S8: *Absorption spectra of rhodamine 6G dye solution: (a) under UV irradiation at different times (inset shows the determination of dye decomposition first order rate constant) using ZSV-LC as photocatalyst, (b) adsorption behaviour of the dye for ZSV-HC at different time and (c) photodegradation of the dye after 60 min of UV exposure.*

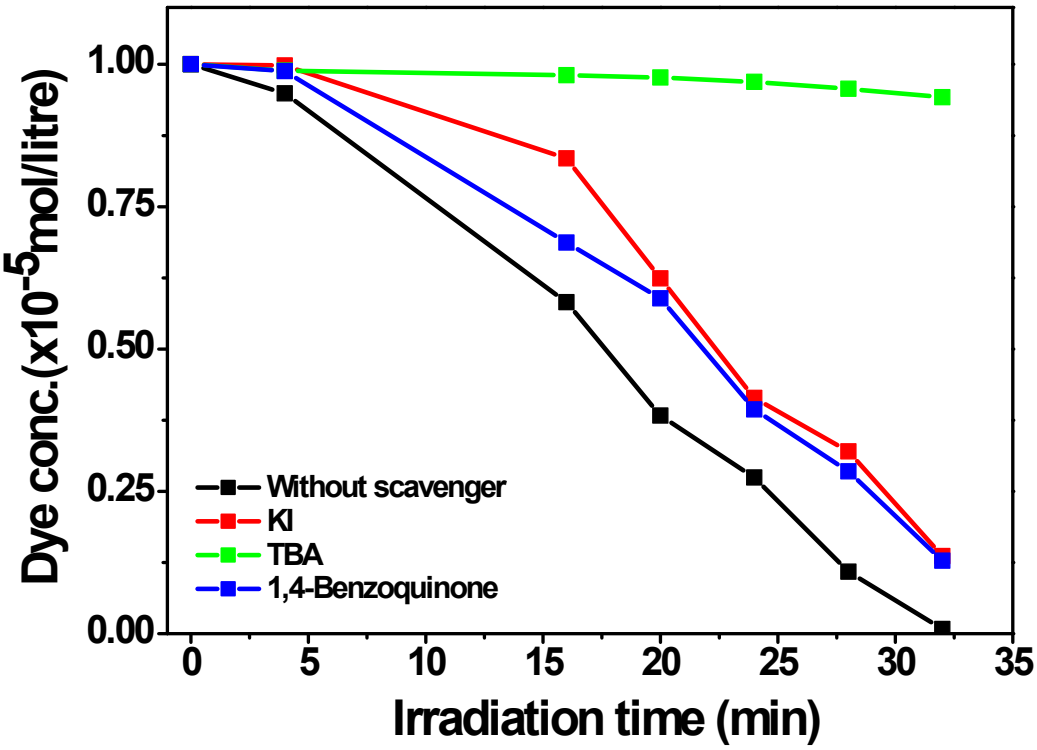

Fig. S9: *Remnant dye concentration versus UV illumination time for the dye solution containing different scavengers for photogenerated charges. KI and TBA indicate potassium iodide and tertiary butyl alcohol, respectively.*